Article

Degradation of Organic Dyes Using the Ionizing Irradiation Process in the Presence of the CN/CD₃/Fe₆ Composite: Mechanistic Studies

Wen Li,[§] Qi Ye,[§] Tao Xia, Long Zhao,* and Miao Yang*

Read Online

ACCESS | 📊 Metrics & More | 📰 Article Recommendations | SI Supporting Information

ABSTRACT: Organic dyes are ubiquitous pollutants in various aquatic environments as they are produced in abundance and used widely. In the present work, the degradation and mineralization of various organic dyes such as methylene blue (MB), methyl orange (MO), and rhodamine B (RhB), following the electron beam irradiation method in the presence of a graphitic carbon nitride/carbon nanodots/Fe(II) (CN/CD₃/Fe₆) composite, were studied. The removal efficiency of MB reached 81.7% under conditions of electron beam irradiation (EBI) when the total irradiation dose was 5 kGy. This increased to 91.2% in the presence of the CN/CD₃/Fe₆ composite. The mineralization efficiency increased from 30.1 to 47.3% when the composite was added, and the total irradiation dose was 20 kGy. The removal efficiency of organic dyes was not significantly affected in the pH range of 3−11. Results from cyclic experiments conducted using MB degradation indicated that the CN/CD₃/Fe₆ composite exhibited good stability and reusability even after

five irradiation cycles. Results from scavenging experiments revealed that $^\bullet$OH was the predominant reactive species during the MB degradation process. Intermediates produced in the synergistic system (EBI&CN/CD₃/Fe₆ system) consisting of the CN/CD₃/Fe₆ composite and EBI were detected using the liquid chromatography-mass spectrometry (LC-MS) technique. Based on the results, the possible degradation mechanism and pathways for MB were proposed.
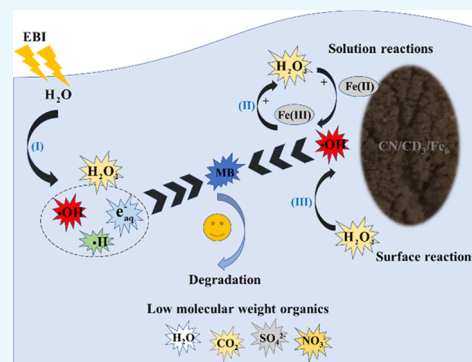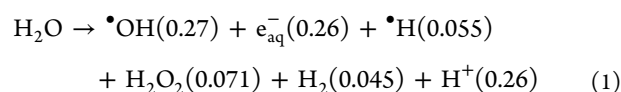
1. INTRODUCTION

With the rapid development of the economy, industrial and agricultural water demand has increased. As a result, water pollution is becoming increasingly prominent. Tons of stable and persistent organic dyes are discharged annually by the textile, dyeing, and paper industries.[1,2] This poses a risk to aquatic organisms and human beings. Hence, it is important to develop efficient dye treatment methods.[3]

Advanced oxidation processes (AOPs) are one of the promising technologies characterized by high degradation and mineralization efficiency for removing pollutants from water. Fenton oxidation, persulfate oxidation, ultrasonication, photocatalysis, ionizing irradiation, and other combined processes are associated with AOPs.[4−7] Ionizing irradiation is an alternative technology used for treating wastewater. Electron beam irradiation (EBI) is an ionizing irradiation technique, and it is a rapid, efficient, and nonselective treatment method. Both oxidants ($^\bullet$OH, H_2O_2) and reductants (e_{aq}^-, $^\bullet$H, H_2) can be produced through water radiolysis (eq 1), and these can degrade the target contaminants. The values in the brackets represent the radiation chemical yield (*G*-value) of each species (expressed in μmol/J) (including gamma ray and electron beam).[8,9] However, it is worth mentioning that the safety issues about EBI and high cost of investment and operation are the main factors limiting its application. Besides, the intermediates produced during the EBI process require higher energy to mineralize. To improve the mineralization

efficiency of organic pollutants and reduce operating costs, EBI is usually applied with addition of some oxidants like H_2O_2, ozone, persulfate, and the metal catalysts such as Fe^{2+} and TiO_2.[10−12]

$$H_2O \rightarrow {}^\bullet OH(0.27) + e_{aq}^-(0.26) + {}^\bullet H(0.055)$$
$$+ H_2O_2(0.071) + H_2(0.045) + H^+(0.26) \quad (1)$$

Composites formed by graphitic carbon nitride (g-C_3N_4)/carbon nanodots (CDs) doped with metals have been extensively studied. These exhibit excellent photocatalytic efficiency during the process of organic pollutant degradation (dye and antibiotic).[13−15] g-C_3N_4 is a low-cost photocatalyst capable of generating H_2 and H_2O_2 from water, and CDs exhibit high catalytic activity during H_2O_2 decomposition. Liu et al. demonstrated that the combination of g-C_3N_4 and CDs exhibited a synergism on the processes of H_2O_2 decomposition and $^\bullet$OH production in the absence of light irradiation.[16] Moreover, the doping of metals and metal oxides can further
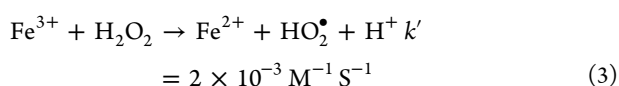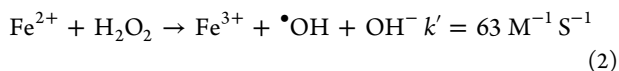
catalyze the degradation of organic pollutants. Chen et al. prepared the composite formed by g-C$_3$N$_4$/CDs doped with metal oxides. They demonstrated that the composite significantly enhanced photodegradation activity toward organic dyes RhB and MB.[17] Fang et al. proposed the composite formed by graphitic carbon nitride/carbon nanodots doped with ferrous ions. They reported that the composite could significantly improve the organic dye removal efficiency under the Haber−Weiss reaction conditions to promote the generation of $^\bullet$OH and HO$_2{}^\bullet$ (eqs 2 and 3).[18] The composite is cost-efficient, can be easily prepared, and exhibits good cyclic degradation performance for organic dyes.[19] This illustrates the excellent catalytic efficiency of the g-C$_3$N$_4$/CD composites doped with metals.

$$Fe^{2+} + H_2O_2 \rightarrow Fe^{3+} + {}^\bullet OH + OH^- \quad k' = 63 \text{ M}^{-1}\text{S}^{-1} \tag{2}$$

$$Fe^{3+} + H_2O_2 \rightarrow Fe^{2+} + HO_2{}^\bullet + H^+ \quad k'$$
$$= 2 \times 10^{-3} \text{ M}^{-1}\text{S}^{-1} \tag{3}$$

It is noticeable that numerous researchers have studied the process of removal of organic pollutants in homogeneous systems following the ionizing irradiation process.[20−23] However, compared with homogeneous systems, a few studies have focused on heterogeneous systems. Yang et al. proposed a method using a combination of Fe/C nanomaterials and the ionizing irradiation method that could be used in the field of antibiotics degradation.[11] Ma et al. demonstrated the degradation of organic dyes using the synergistic system consisting of g-C$_3$N$_4$ and ionizing irradiation.[24] Chen et al. studied the degradation characteristic and mineralization efficiency of norfloxacin by ionizing irradiation technology combined with Fenton-like oxidation (magnetite and goethite).[25] The high organic pollutant removal efficiencies were emphasized in all of the above reports. This suggested that ionizing irradiation could be potentially used for the degradation of organic pollutants present in heterogeneous systems. However, the reaction mechanism (for surface and solution reactions) associated with heterogeneous irradiation systems (the synergistic system consisting of a heterogeneous catalyst and ionizing irradiation) was not studied in these reports. Herein, the reaction mechanism associated with the system for a high concentration of organic dyes has been discussed in detail.

The degradation and mineralization of organic dyes in the synergistic system (EBI&CN/CD$_3$/Fe$_6$ system) consisting of the CN/CD$_3$/Fe$_6$ composite and EBI were studied. The paper reports the (a) efficiencies of the EBI system and homogeneous and heterogeneous EBI&CN/CD$_3$/Fe$_6$ systems used for the degradation and mineralization of organic dyes, (b) influence of solution pH, (c) stability and reusability of the CN/CD$_3$/Fe$_6$ composite, (d) main reactive species involved, (e) intermediates formed, and (f) degradation mechanism and pathways. New ideas for efficient degradation and mineralization of organic dyes have been proposed.

2. EXPERIMENTAL SECTION

2.1. Materials. Methylene blue trihydrate (MB, CAS [7220-79-3], ≥82.0%), rhodamine B (RhB, CAS [81-88-9], AR, ≥98%), methyl orange (MO, CAS [547-58-0], ≥98.5%), urea (CAS [57-13-6], ≥99%), citric acid monohydrate (CAS [5949-29-1], ≥99.5%), iron(II) sulfate heptahydrate (CAS

[7782-63-0], 99.0−100.0%), sodium hydroxide (CAS [1310-73-2], AR, ≥96%), hydrochloric acid (CAS [7647-01-0], GR), and sodium formate dihydrate (CAS [141-53-7], AR) were obtained from Sinopharm Chemical Reagent Co., Ltd. *Tert*-butanol (CAS [75-65-0], AR, ≥99%) was obtained from Shanghai Macklin Biochemical Co., Ltd. Ultrapure water obtained from the EASY Ultrapure Water System (HealForce) was used for all of the studies.

2.2. Synthesis of the CN/CD$_3$/Fe$_6$ Composite. Citric acid (1.5 g) and urea (50 g) were mixed evenly into a crucible. The mixture was calcined at 550 °C for 3 h at a rate of 1 °C/min in a muffle furnace. Following this, it was cooled to room temperature (about 25 °C). Subsequently, the samples were washed, dried, and ground to obtain CN/CD$_3$. The CN/CD$_3$ solid powder (1.2 g) was mixed with 300 mL of 6 mM FeSO$_4$ solution, and the mixture was stirred evenly. Following this, the mixture was ultrasonically dispersed into the suspension over 25 min. The mixture was stirred at a constant temperature of 60 °C to obtain the dried sample. The obtained sample was ground to form powder to obtain the target CN/CD$_3$/Fe$_6$ composite.[19]

2.3. EBI Experiments. All irradiation processes were carried out using a 0.4 MeV electron accelerator (dose per pass: 0.84 kGy/pass) in the State Key Laboratory of Advanced Electromagnetic Engineering and Technology, School of Electrical and Electronic Engineering, Huazhong University of Science and Technology. The high voltage was set as 400 kV, and the current of electron beam was 2.1 mA in every pass. The speed of the conveyor was 10 m/min. The experiment of total organic carbon (TOC) was carried out using a 1.0 MeV electron accelerator (dose per pass: 5 kGy/pass) in the School of Hubei University of Science and Technology. The dose was measured by an FWT-60-00 film color developer dose tablet. All irradiation treatments were conducted in duplicate at room temperature. In the EBI&CN/CD$_3$/Fe$_6$ system, the CN/CD$_3$/Fe$_6$ composite was spiked into organic dyes to reach the conditions of adsorption equilibrium before irradiation (according to the preliminary experiments, adsorption equilibrium can be reached because of the adequate adsorption time). The irradiated samples (5 mL) were filtered using 0.22 μm syringe filters for further use.

2.4. Analytical Methods. The ultraviolet−visible spectroscopy (UV/vis) profiles were recorded using a UV-2700 system (Shimadzu, Japan). The profiles were analyzed to detect the concentration of the organic dyes. The absorption wavelengths corresponding to MB, MO, and RhB were determined to be 665, 464, and 554 nm, respectively, by scanning the maximum absorption peak. The three dyes were diluted within the standard curve range of 0−10 mg/L, and it was observed that the absorbance was closely related to the concentration of the organic dyes ($R^2 > 0.99$). The TOC values of the organic dyes were determined using a TOC analyzer (HTY-CT1000B, China). The organic dye solutions were processed using the heavy metal digestion instrument from Hanon (SH230N, China). The iron ion concentration was detected using the inductively coupled plasma-optical emission spectrometry (ICP-OES) technique. The system used was obtained from Agilent Technologies Inc. (Agilent 5110). The specific surface area of the CN/CD$_3$/Fe$_6$ composite was determined by the Brunauer−Emmet−Teller (BET) method through the isothermal adsorption and desorption of high-purity N$_2$ using a TriStar II 3020 analyzer (Micromeritics).
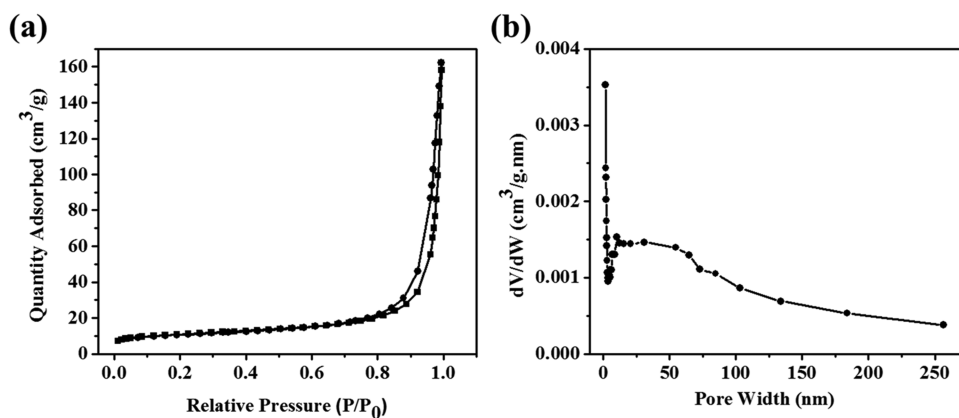
Figure 1. (a) Nitrogen adsorption−desorption isotherm and (b) pore-size distribution of the $CN/CD_3/Fe_6$ composite.
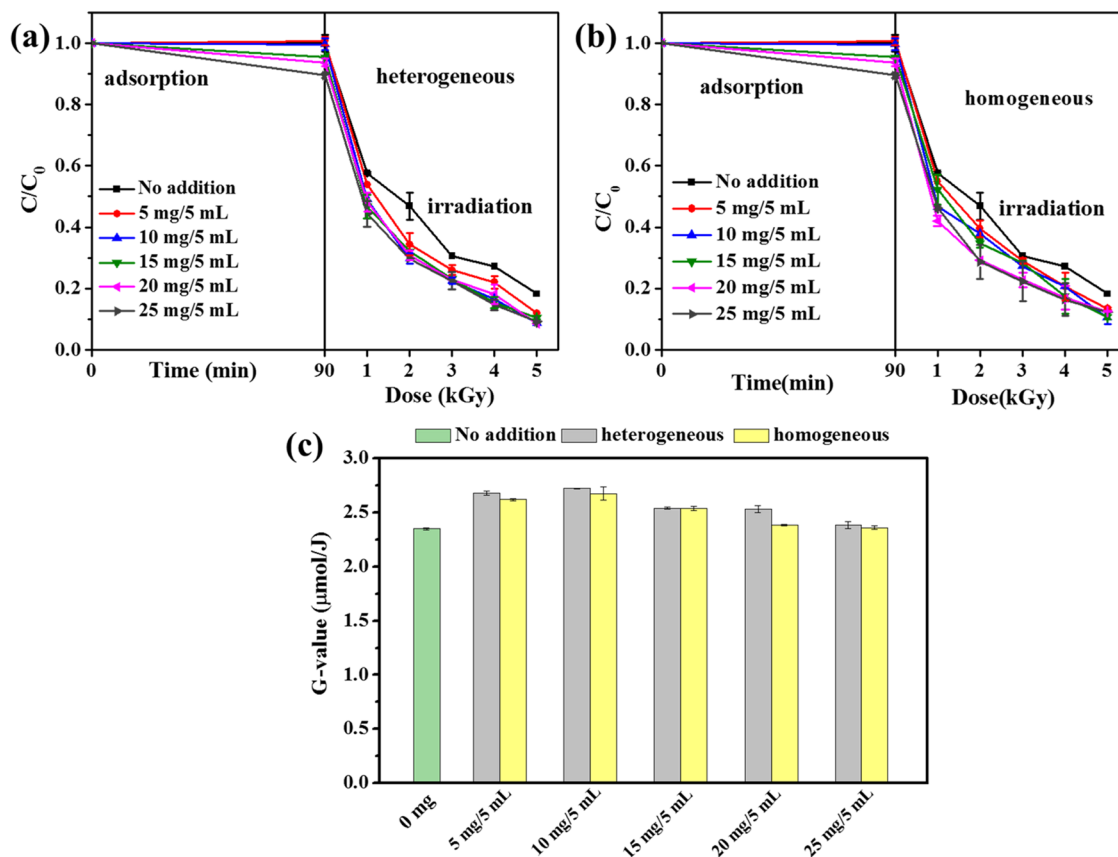

Figure 2. Effect of the $CN/CD_3/Fe_6$ composite dosage on the MB degradation efficiency in the $EBI\&CN/CD_3/Fe_6$ system: (a) heterogeneous irradiation, (b) homogeneous irradiation, and (c) comparison of G-value (dose: 5 kGy), $[MB]_0 = 500$ mg/L, pH = 5.3.

The physiochemical properties of the $CN/CD_3/Fe_6$ composite before and after EBI experiments were characterized using transmission electron microscopy (TEM), X-ray diffraction (XRD), Fourier transform infrared spectroscopy (FTIR), and X-ray photoelectron spectroscopy (XPS) techniques. The morphology was examined using a 200 kV TEM instrument purchased from JEOL (JEM-2100F, Japan). The crystal structure and phase were determined using an XRD instrument obtained from PANalytical B.V. (Empyrean, The Netherlands) (using Cu Kα irradiation (λ = 1.54 Å) in the 2θ range between 10 and 70° with a 0.013° step size), and the XRD data were processed using MDI Jade 6.5 software. The crystallite size was calculated by the Debye−Scherrer equation (eq 4).

$$D = \frac{K\lambda}{B \cos \theta} \tag{4}$$

where the crystallite size is denoted by D, the shape factor is denoted by K ($K = 0.9$), the wavelength of Cu Kα irradiation is denoted by λ (λ = 0.154 nm), the FWHM of the sample diffraction peak is denoted by B, and the diffraction angle is denoted by θ. The functional group was identified using an FTIR machine obtained from Thermo Fisher Scientific (Nicolet 6700). The elemental composition and chemical states were analyzed using the XPS technique (Thermo Fisher Scientific, ESCALAB 250Xi). To neutralize the charge of the sample, the flood gun was used to improve the charging effect using the charging compensation. All peaks were calibrated
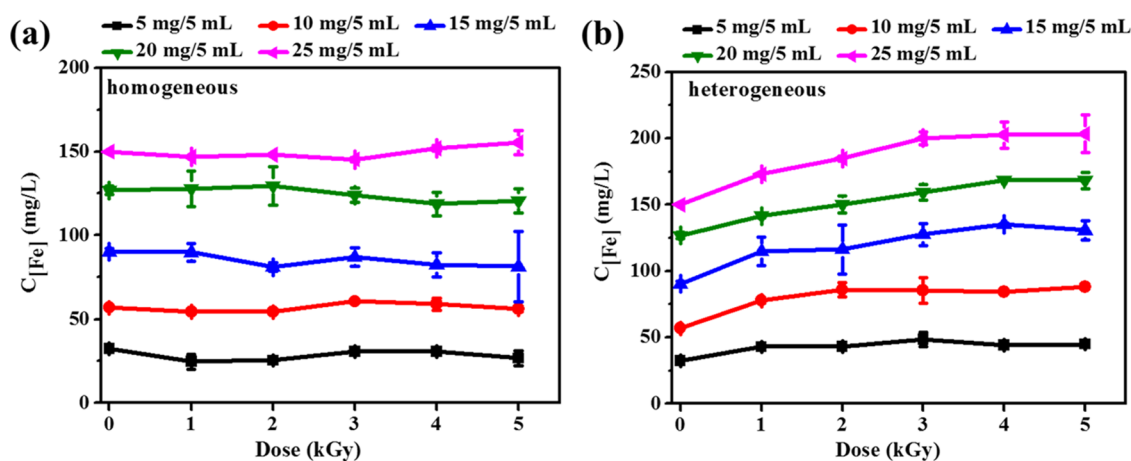
Figure 3. Concentration of iron ions in the EBI&CN/CD$_3$/Fe$_6$ system under conditions of (a) homogeneous irradiation and (b) heterogeneous irradiation. $[MB]_0$ = 500 mg/L, pH = 5.3.
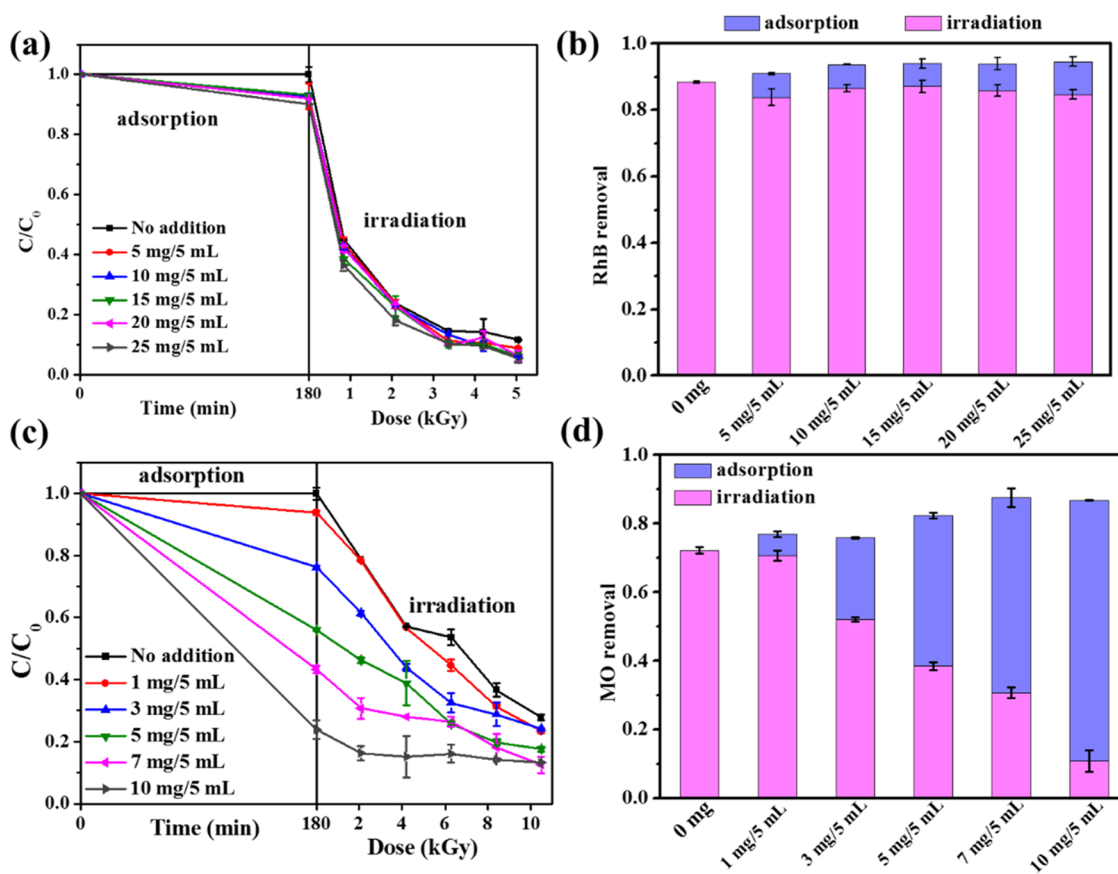

Figure 4. Effect of the CN/CD$_3$/Fe$_6$ composite dosage on (a, b (dose: 5 kGy)) RhB and (c, d (dose: 10.5 kGy)) MO degradation in the EBI&CN/CD$_3$/Fe$_6$ system under conditions of heterogeneous irradiation. $[RhB]_0$ = 1000 mg/L, pH = 3.5. $[MO]_0$ = 1000 mg/L, pH = 6.5.

against the C 1s peak at 284.8 eV,[26] and the XPS data were processed using XPSPEAK41 software.

The irradiated samples were filtered using 0.22 μm syringe filters to filter out the CN/CD$_3$/Fe$_6$ composite. After that, the irradiated samples were put in an electric blast drying oven at 50 °C to concentrate them. Finally, the processed MB solution was identified using a high-performance liquid chromatography system obtained from Thermo Fisher Scientific (UltiMate 3000) and the mass spectrometer obtained from Bruker Daltonics Inc. (micrOTOF II, Germany). The LC-MS system was equipped with a Boston Green ODS LC column (5 μm,

4.6 × 250 mm^2). The analysis was carried out under the electrospray ionization ion operating mode (positive). The mobile phase of MB consisted of a mixture of methanol and water (3:97, v/v). The flow rate was maintained at 1.0 mL min^{-1}, the injected volume was 20 μL, and the temperature for the detector was kept at 25 °C.

3. RESULTS AND DISCUSSION

3.1. BET Analysis of the CN/CD$_3$/Fe$_6$ Composite. The specific surface area and the pore-size distribution of the CN/CD$_3$/Fe$_6$ composite were calculated through the isothermal
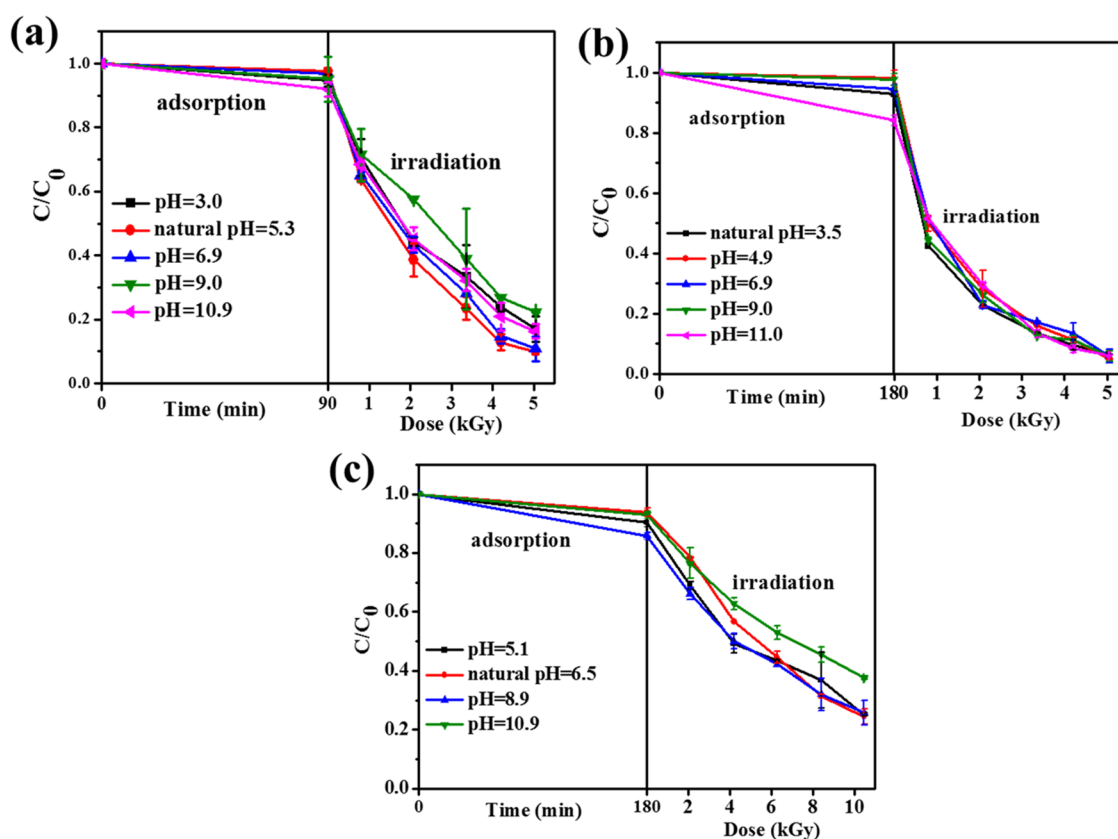
Figure 5. Effect of solution pH on (a) MB, (b) RhB, and (c) MO degradation in the EBI&CN/CD$_3$/Fe$_6$ system under conditions of heterogeneous irradiation. $[MB]_0$ = 500 mg/L, $[CN/CD_3/Fe_6]$/V(MB) = 10 mg/5 mL. $[RhB]_0$ = 1000 mg/L, $[CN/CD_3/Fe_6]$/V(RhB) = 10 mg/5 mL. $[MO]_0$ = 1000 mg/L, $[CN/CD_3/Fe_6]$/V(MO) = 1 mg/5 mL.

adsorption/desorption of high-purity nitrogen using the BET method (Figure 1). The CN/CD$_3$/Fe$_6$ composite showed type IV and H3-type hysteresis loops (Figure 1a), indicating the presence of mesopore structures. The Barrett−Joyner−Halenda pore-size distributions of the CN/CD$_3$/Fe$_6$ composite verified the assumption, and the pore sizes were mainly distributed below 20 nm (Figure 1b).[27,28] The results suggested that the calculated specific surface area and the average pore diameter of the CN/CD$_3$/Fe$_6$ composite were 37.40 m^2 g^{-1} and 20.98 nm, respectively. The specific surface area is higher than some reported g-C$_3$N$_4$-based materials.[29,30] The porous structures and large specific surface area can provide more active sites for pollutant adsorption and degradation.

3.2. Degradation of Organic Dyes Using the EBI&CN/CD$_3$/Fe$_6$ System. *3.2.1. Effect of Heterogeneous and Homogeneous Irradiation Systems on the Process of MB Degradation.* The effect of heterogeneous and homogeneous irradiation systems on the process of degradation of MB was investigated (Figure 2). It is noticeable that the irradiation process started after adsorption equilibrium was reached in the presence of the CN/CD$_3$/Fe$_6$ composite and MB solution (adsorption equilibrium of MB was reached at 90 min during the preliminary experiment). The purpose of performing experiments under conditions of both the heterogeneous and homogeneous (filtering the heterogeneous solution containing the composite and MB before irradiation, unfiltered CDs, and dissolved iron species present in the solution) irradiation systems is to verify the presence of solution reaction and its contribution to the process of MB degradation. The ICP-OES

technique was used to measure the concentration of the dissolved iron species to understand the process of leaching of iron ions and the reaction mechanism (Figure 3).[19]

Figure 2 shows the process of degradation of MB under conditions of different systems, and the normalized concentration (C/C_0) was plotted against the irradiation dose (Figure 2a,b).

The MB removal efficiency of the EBI system was significantly lower than the MB removal efficiency of the system containing the CN/CD$_3$/Fe$_6$ composite. To be more specific, the removal efficiency of MB under conditions of EBI reached 81.7% at 5 kGy. The value increased to 89.6% under homogeneous irradiation and 91.2% under heterogeneous irradiation conditions. The results obtained using a homogeneous irradiation system were better than those obtained using the EBI system alone. This implied the existence of solution reactions. Although there was no statistically significant difference between the heterogeneous irradiation system and the homogeneous irradiation system (Figure 2c), the MB removal efficiency and *G*-value between the two systems still had a slight difference, and it is speculated that there may also be surface reactions in the heterogeneous irradiation system. The optimal solid−liquid ratio was found to be 10 mg/5 mL. This could be attributed to the highest removal efficiency and *G*-value recorded during the process of MB degradation. Further experiments for MB degradation will be carried out based on the optimal solid−liquid ratio.

The iron ion concentration ($C_{[Fe]}$) in the EBI&CN/CD$_3$/Fe$_6$ system is presented in Figure 3. As can be seen, the $C_{[Fe]}$ recorded in the homogeneous irradiation system remained
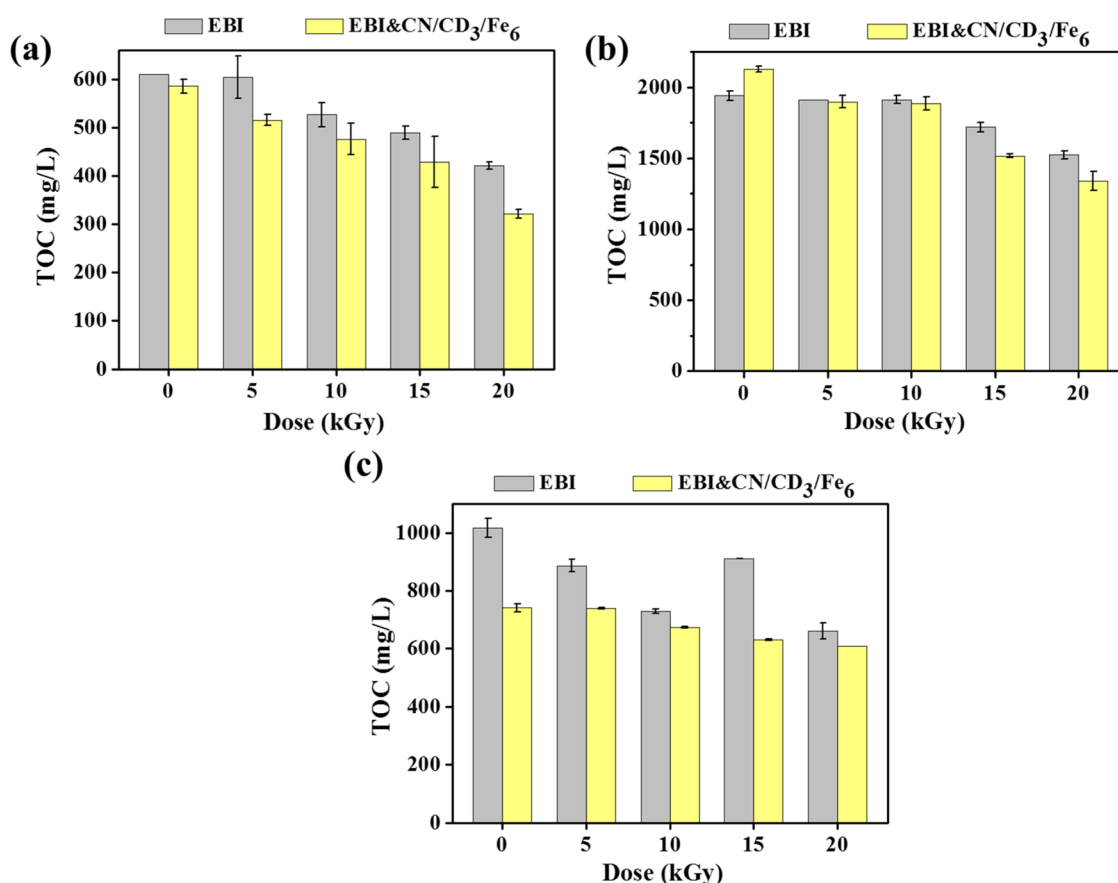
Figure 6. TOC values recorded for (a) MB, (b) RhB, and (c) MO solutions in the EBI system and EBI&CN/CD$_3$/Fe$_6$ systems under conditions of heterogeneous irradiation. $[MB]_0$ = 1000 mg/L, $[CN/CD_3/Fe_6]$/V(MB) = 20 mg/5 mL, pH = 5.3. $[RhB]_0$ = 2000 mg/L, $[CN/CD_3/Fe_6]$/V(RhB) = 20 mg/5 mL, pH = 3.5. $[MO]_0$ = 1000 mg/L, $[CN/CD_3/Fe_6]$/V(MO) = 1 mg/5 mL, pH = 6.5.

stable (Figure 3a) and that recorded in the heterogeneous irradiation system increased (Figure 3b) with an increase in the irradiation dose. The phenomenon could be attributed to the reaction mechanism and can be explained primarily on the basis of various aspects. (1) The $C_{[Fe]}$ in the homogeneous system remained stable, but the removal efficiency of MB recorded for the homogenous system was higher than that recorded for the EBI system devoid of additives (Figure 2b). This indicated that there were reactions that did not consume dissolved iron present in the solution. This can be attributed to the Haber−Weiss reactions (eqs 2 and 3), and the H$_2$O$_2$ (produced in situ during the process of water radiolysis) and iron species in the solution trigger the continuous generation of the •OH and HO$_2$• radicals.[18] In addition, the remaining CDs in the filtered solution can catalyze the decomposition of H$_2$O$_2$ to generate •OH. It may also be contributing factors for MB degradation.[19] (2) The $C_{[Fe]}$ recorded for the heterogeneous irradiation system increased, and this could be attributed to the leaching of iron ions occurring during the irradiation process. The MB removal efficiency and G-value between the heterogeneous irradiation system and the homogeneous irradiation system were slightly different; this may be because both the solution and surface reactions occurred in the heterogeneous irradiation system. On the one hand, iron ions leached into the heterogeneous irradiation system. This enhanced the solution reactions. On the other hand, H$_2$O$_2$ (produced in situ during the process of water radiolysis) adsorbed on the surface of the CN/CD$_3$/Fe$_6$ composite can be able to react with the CDs of the CN/CD$_3$/Fe$_6$ composite to

trigger the production of the surface-bound •OH radicals. However, a statistically significant difference was not observed between the two systems, and this indicates that the solution reactions play a dominant role during the MB degradation process.

In addition, it is quite clear that while the difference in CN/CD$_3$/Fe$_6$ composite dosage and the connected dissolution of iron differ significantly between the different solutions, the difference in removal efficiency is very small. This phenomenon occurred due to the relatively low content of H$_2$O$_2$ produced through water radiolysis, and CDs in the solutions are also contributing factors for MB degradation.

3.2.2. Degradation of RhB and MO in the Heterogeneous Irradiation System. Besides MB, the degradation of RhB and MO in the heterogeneous irradiation system was also studied. Results from preliminary experiments suggested that both RhB and MO reached adsorption equilibrium at 180 min. As shown in Figure 4, the adsorption performance of the CN/CD$_3$/Fe$_6$ composite for MO was higher than that for RhB. This can be potentially attributed to the strong electrostatic interactions between MO and the CN/CD$_3$/Fe$_6$ composite.[31] During the irradiation process, the maximum removal efficiencies of RhB and MO reached 94.5 and 87.5%, respectively. It should be noted that the removal efficiency for RhB and MO in the heterogeneous irradiation system was higher than those recorded for the EBI system alone.

In addition, based on the contribution of adsorption and irradiation in dye removal (eqs 5−7), the solid−liquid ratio when the irradiation contribution was the largest was selected
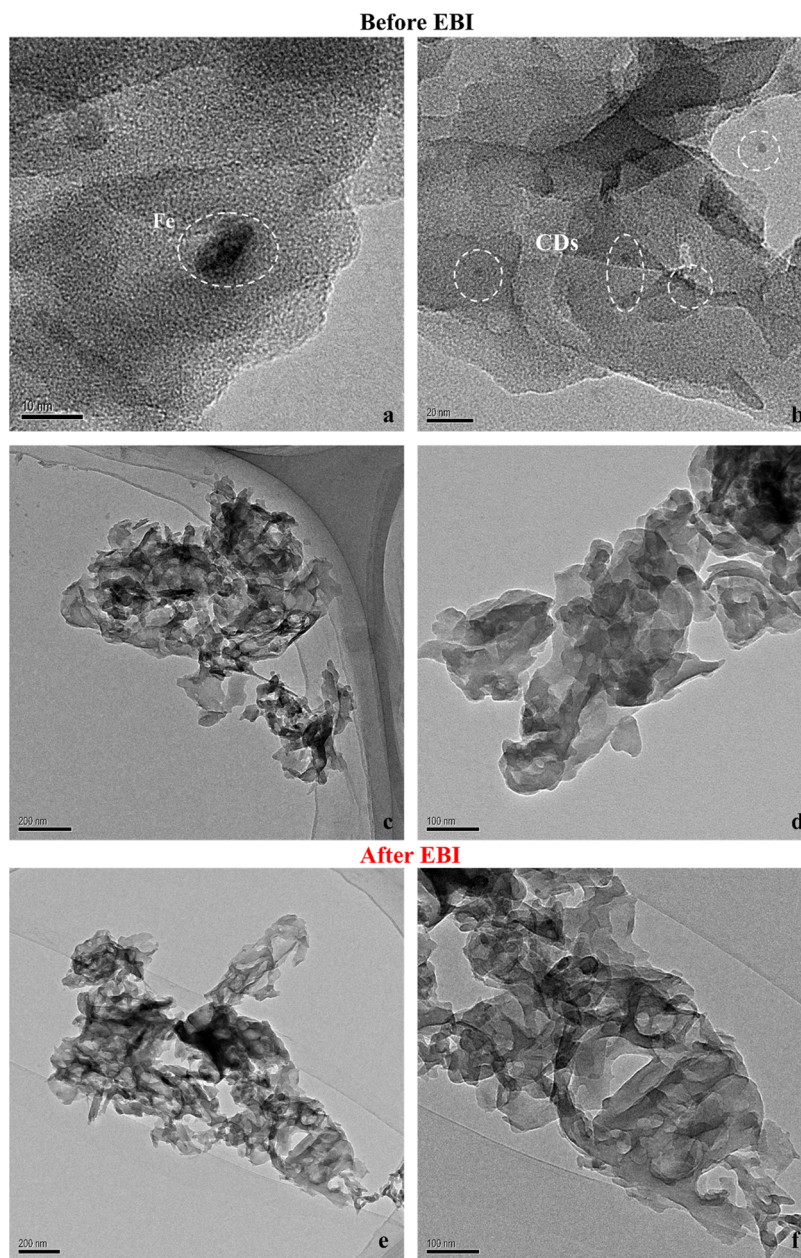
Before EBI

After EBI

Figure 7. TEM images recorded for the $CN/CD_3/Fe_6$ composite: fresh (a–d) and after five times of irradiation (e, f).

as the optimal solid−liquid ratio from the study point of view.[11]

$$\text{removal efficiency} = \frac{C_0 - C_2}{C_0} \quad (5)$$

$$\text{adsorption contribution} = \frac{C_0 - C_1}{C_0} \quad (6)$$

$$\text{irradiation contribution} = \frac{C_1 - C_2}{C_0} \quad (7)$$

where the initial concentration of dye is denoted by C_0, the concentration of dye after adsorption was completed is denoted by C_1, and the concentration of dye after the whole process of adsorption and irradiation was completed is denoted by C_2. As shown in Figure 4b,d, the optimal solid−liquid ratios for RhB and MO were determined to be 10 mg/5 mL and 1

mg/5 mL, respectively. Further RhB and MO degradation experiments will be carried out based on the optimal solid−liquid ratio.

3.2.3. Effect of Solution pH on the Process of Organic Dyes Degradation. The effect of initial pH on the process of organic dyes degradation using the $EBI\&CN/CD_3/Fe_6$ system was also explored (Figure 5). It is clear that alkaline conditions are more conducive to the adsorption of MB and RhB. Efficient MO adsorption could not be realized under alkaline conditions (pH = 10.9). This could be attributed to the combined effect of pK_a of MO (3.4) and pH_{pzc} of the $CN/CD_3/Fe_6$ composite (5.5). When the MO solution became strongly alkaline, the adsorption of MO is lower because of ionic interaction between the negatively charged $CN/CD_3/Fe_6$ composite surface and negatively charged MO molecule.[32] The effect of pH on the degradation of the three dyes was not the same during the EBI process. There was a negative impact on
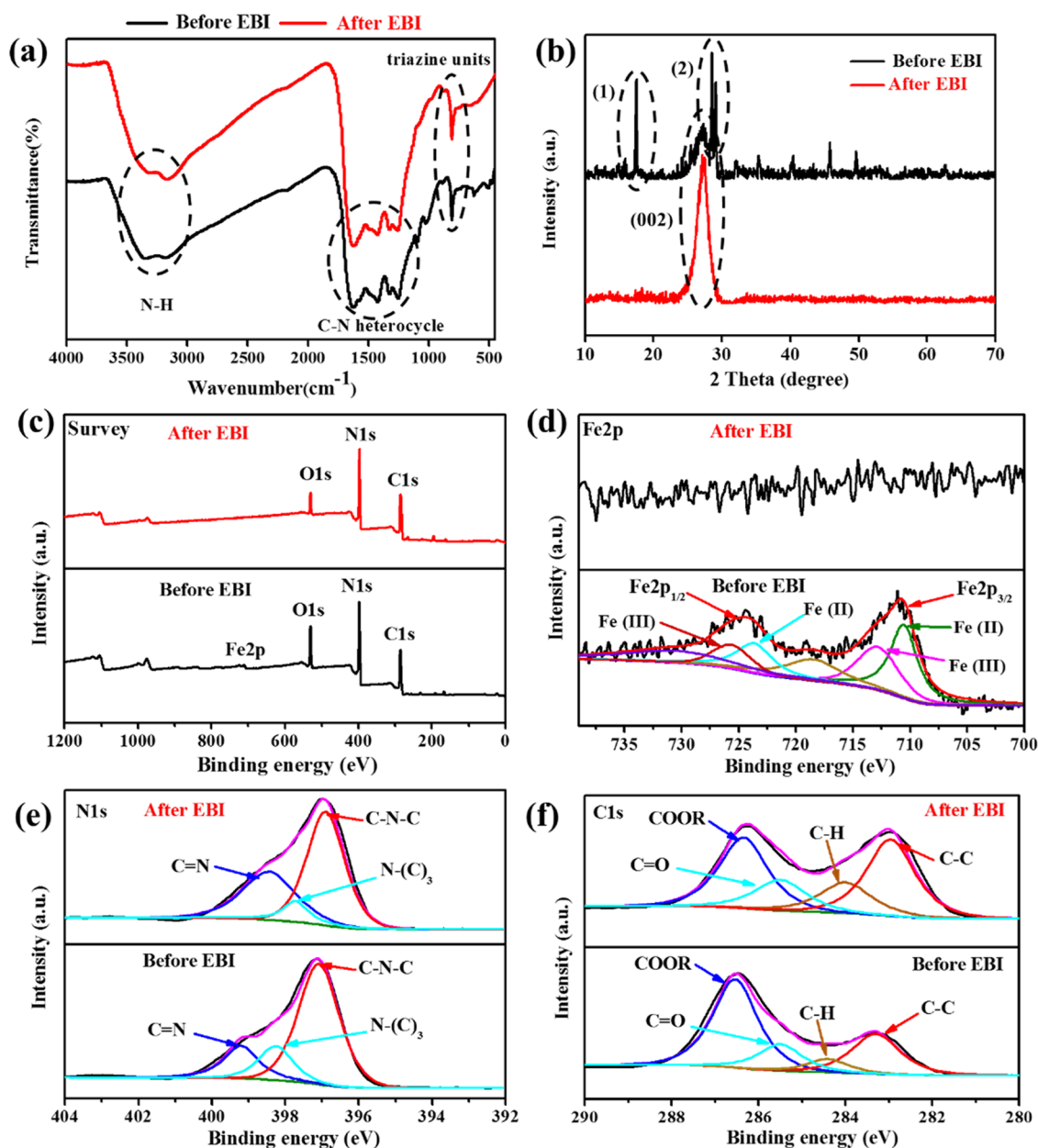
Figure 8. (a) FTIR, (b) XRD, and (c−f) XPS profiles recorded for the CN/CD$_3$/Fe$_6$ composite (before and after five irradiation cycles).

MB degradation under strongly acidic and alkaline conditions. This could be attributed to the reactions of reactive species in the solution.[33] The effect of pH was not obvious during the process of RhB degradation. In the pH range of 3.5−11.0, the removal efficiency of RhB was >93.0%. Under different pH conditions, the removal efficiency of MO reached approximately 75.0% at 10 kGy, but the degradation efficiency decreased at pH = 10.9. This can be attributed to the fact that when the solution is strongly alkaline, the surface charge of the CN/CD$_3$/Fe$_6$ composite and MO repel each other. Thus, the process of MO degradation was hindered.[34]

In general, although different pH-dependent effects were observed for the three dyes within the pH range of 3−11, the efficiency in each case was acceptable. More specifically, MB, RhB, and MO have the lowest efficiency under alkaline conditions and reached 77.6, 93.7, and 62.4%, respectively. It is worth mentioning that the typical Fenton reaction is strictly limited to an impractically low pH (<4) as there is a

production of a large mass of iron precipitates under neutral and alkaline conditions,[35] and the heterogeneous irradiation system studied in this article was not pH limited as the typical Fenton oxidation. In addition, the highest removal efficiency for the three dyes was recorded under natural pH conditions. This can facilitate the practical application of the organic dye treatment method.

3.3. Mineralization of Organic Dyes. TOC is an important indicator of the degree of mineralization for organic matters. In this study, organic dyes were irradiated in two systems to assess the efficiency of TOC removal during the EBI process. The mineralization performance of MB, RhB, and MO in the EBI and EBI&CN/CD$_3$/Fe$_6$ systems is shown in Figure 6.

The EBI&CN/CD$_3$/Fe$_6$ system exhibited a higher TOC removal efficiency for the three dyes compared to the EBI system. This suggested that the synergistic system consisting of EBI and the CN/CD$_3$/Fe$_6$ composite could be used to

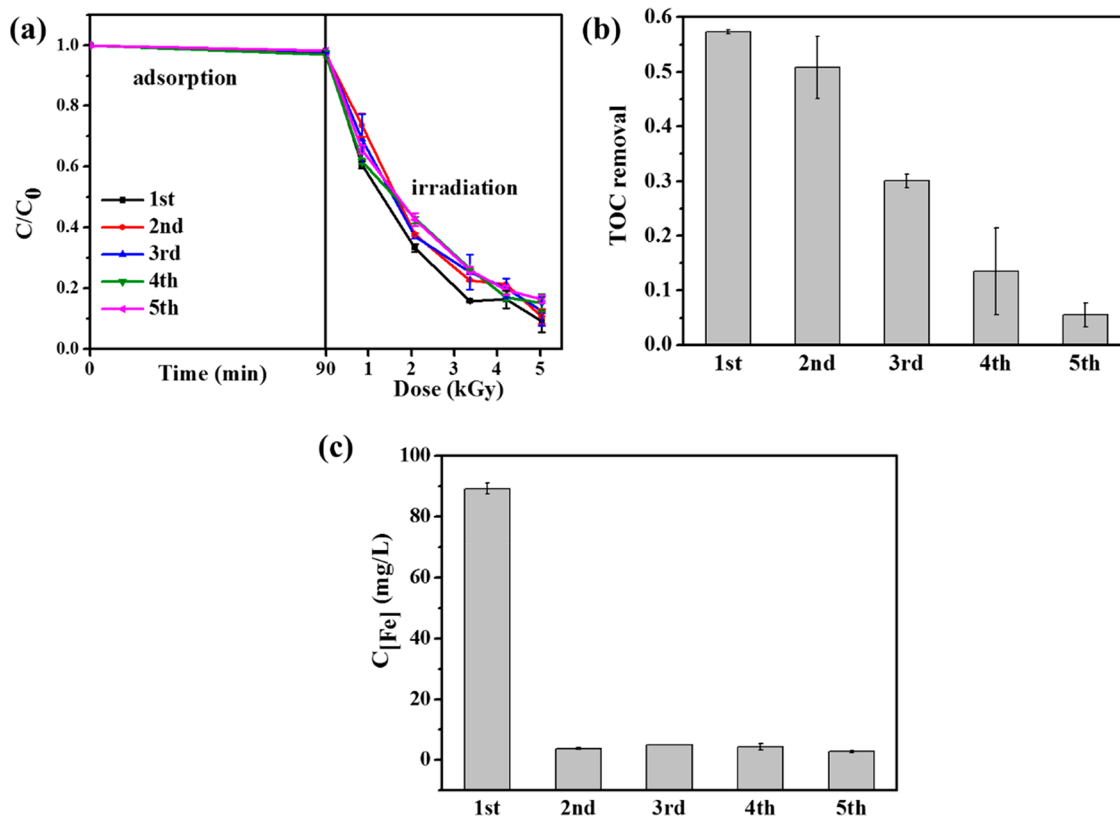**Table 1. Fitting Parameters Obtained by the XPS Spectra: Binding Energy (eV) and Percentage of Total Area (%)**

	core level		energy (eV)	state	%
Fe 2p	before EBI	Fe 2p$_{3/2}$	710.5	Fe(II)	
			712.9	Fe(III)	Fe(II) 56.8
			718.4	Fe(II) satellite	
		Fe 2p$_{1/2}$	723.6	Fe(II)	
			725.7	Fe(III)	Fe(III) 43.2
			730.0	Fe(III) satellite	
	after EBI	none			
N 1s	before EBI		397.1	C−N−C	66.1
			398.3	N-(C)$_3$	16.6
			399.2	C=N	17.3
	after EBI		396.9	C−N−C	56.1
			397.7	N-(C)$_3$	9.5
			398.5	C=N	34.4
C 1s	before EBI		283.0	C−C	25.4
			284.0	C−H	7.3
			285.5	C=O	15.5
			286.4	COOR	51.8
	after EBI		283.3	C−C	35.9
			284.4	C−H	15.5
			285.5	C=O	15.5
			286.5	COOR	33.1

improve the decomposition of organic dyes and increase the removal efficiency of organic content in the solution. The

Table 2. Major Reactive Species under Different Experimental Conditions

experiment conditions	major reactive species
N$_2$ saturated	$^{\bullet}$OH, e$_{aq}^-$, $^{\bullet}$H
N$_2$ saturated + TBA	e$_{aq}^-$, $^{\bullet}$H
N$_2$ saturated + formate	e$_{aq}^-$
O$_2$ saturated	$^{\bullet}$OH
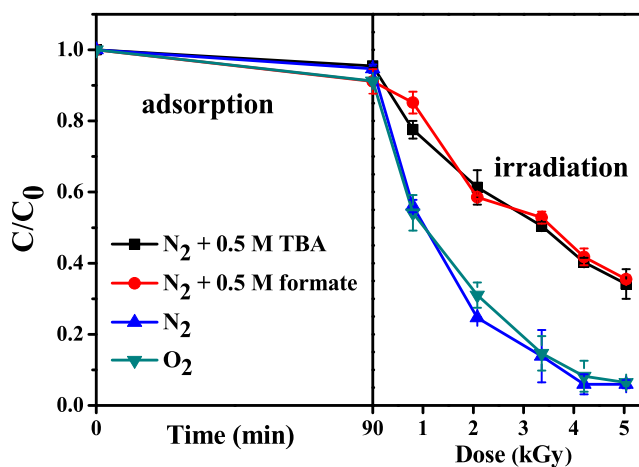
Figure 10. Degradation of MB in the EBI&CN/CD$_3$/Fe$_6$ system under conditions of heterogeneous irradiation under different atmospheric conditions in the presence and absence of scavengers. [MB]$_0$ = 500 mg/L, [TBA] = 0.5 M, [Formate] = 0.5 M. [CN/CD$_3$/Fe$_6$]/V(MB) = 10 mg/5 mL, pH = 5.3.

Figure 9. Cyclic experiments conducted using the CN/CD$_3$/Fe$_6$ composite in the EBI&CN/CD$_3$/Fe$_6$ system under conditions of heterogeneous irradiation. (a) Degradation of MB. [MB]$_0$ = 500 mg/L, [CN/CD$_3$/Fe$_6$]/V(MB) = 10 mg/5 mL, pH = 5.3, (b) TOC removal in MB solution [MB]$_0$ = 1000 mg/L, [CN/CD$_3$/Fe$_6$]/V(MB) = 20 mg/5 mL, pH = 5.3, (irradiation dose: 25 kGy), and (c) iron ion concentration.
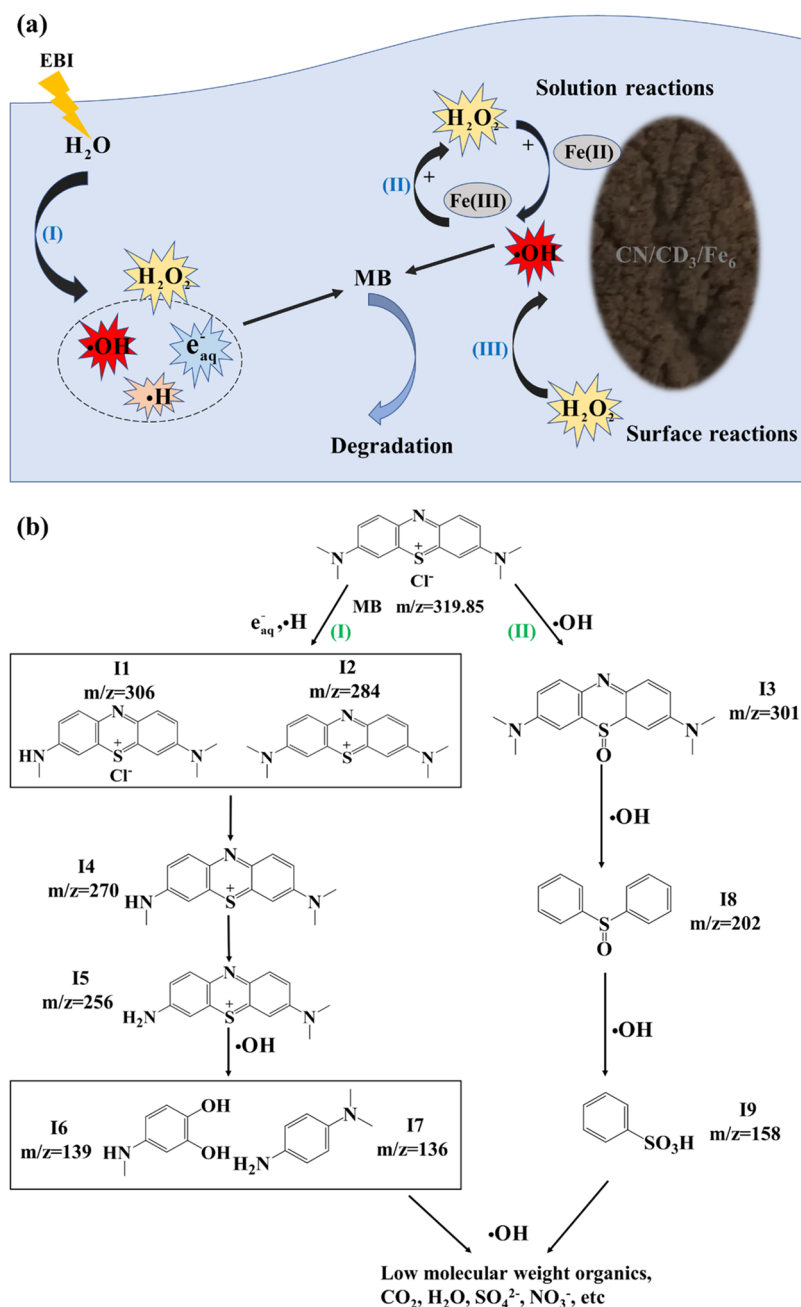
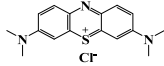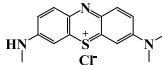**Figure 11.** Degradation (a) mechanism and (b) pathways of MB in the EBI&CN/CD$_3$/Fe$_6$ system.
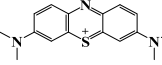
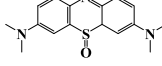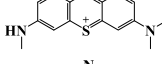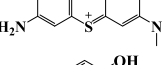TOC value gradually decreased with an increase in the irradiation dose (for the three dyes in the two systems). The increased TOC value for MO at 15 kGy in the EBI system can be potentially attributed to the byproducts produced during the irradiation process.[36] The TOC value for RhB at 0 kGy in the EBI&CN/CD$_3$/Fe$_6$ system was higher than that recorded for the EBI system alone. This can be attributed to the remaining CDs in the filtered solution.

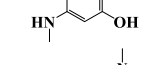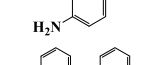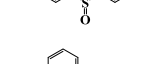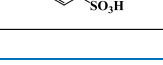**3.4. Cyclic Experiment Using the CN/CD$_3$/Fe$_6$ Composite for MB Degradation.** Five cycles of MB degradation tests were performed to evaluate the stability and reusability of the CN/CD$_3$/Fe$_6$ composite. Following the process of EBI treatment, the CN/CD$_3$/Fe$_6$ composite was collected, washed, and dried. Following this, they were reutilized for the next irradiation experiment.

3.4.1. Characterization of the CN/CD$_3$/Fe$_6$ Composite. Characterization tests were performed using fresh and five-time irradiated CN/CD$_3$/Fe$_6$ composites, and the TEM, FTIR, XRD, and XPS techniques were used for sample characterization.

Analysis of the TEM images (Figure 7) revealed that the presence of iron (Figure 7a) and the random distribution of CDs on the CN/CD$_3$/Fe$_6$ composite (Figure 7b) could also be observed. The morphology of the CN/CD$_3$/Fe$_6$ composite before irradiation (Figure 7c,d) is consistent with previous works.[19] The morphology of the CN/CD$_3$/Fe$_6$ composite hardly changed after five irradiation cycles (Figure 7e,f). This suggested that the CN/CD$_3$/Fe$_6$ composite remained stable after irradiation. This is beneficial for the process of reutilization.

Table 3. Degradation Products of MB Identified by LC-MS

MB (319.85)	intermediates	Chemical structure	m/z
	I1		306
	I2		284
	I3		301
	I4		270
	I5		256
	I6		139
	I7		136
	I8		202
	I9		158

The FTIR spectral profiles of the $CN/CD_3/Fe_6$ composite before and after irradiation were recorded (Figure 8a). The peak appearing at 810 cm^{-1} represented the characteristic stretching vibration mode of the triazine units. The peaks in the region of 1200−1650 cm^{-1} were assigned to the stretching vibration of the C−N heterocycle, and the broad absorption bands appearing in the region of 3000−3500 cm^{-1} represented the stretching vibrational modes of the N−H units of the uncondensed amino groups.[19,37] The position of the characteristic peak of the $CN/CD_3/Fe_6$ composite remained unchanged. This indicated that the functional group was stable after irradiation.

The XRD patterns (Figure 8b) exhibited the presence of three peaks at 17.5, 27.3, and 29° before irradiation. The crystallite size calculated by the Debye−Scherrer equation was 2.61 nm. The peak at 27.3° corresponded to the (002) planes of g-C_3N_4,[38,39] and the intensities of the (002) g-C_3N_4 peak increased after irradiation. This can be potentially attributed to the decrease in the iron content on the surface of the $CN/CD_3/Fe_6$ composite.[40] The peaks at 17.5° (1) and 29° (2) corresponded to the diffraction peaks of compounds containing Fe(II) and Fe(III), and the results were in agreement well with the PDF no. 36-0425 strand card. The peaks of iron ions almost disappeared after irradiation, and this could attribute to the leaching of iron ions during irradiation. However, according to the XRD patterns of the $CN/CD_3/Fe_6$ composite, the diffraction peaks related to CDs are absent due to their very low amount.[41]

The surface chemical states of the elements present in the $CN/CD_3/Fe_6$ composite (before and after irradiation) were confirmed using the XPS technique. The peak corresponding to Fe2p (after irradiation) was absent in the spectral profile recorded for the Survey and Fe2p (Figure 8c,d, respectively). Analysis of Figure 8d reveals that Fe(II) and Fe(III) were present on the $CN/CD_3/Fe_6$ composite (before irradiation).

The results agreed well with the results obtained using the XRD technique. These results demonstrate that the Fe(II) species were partially oxidized to Fe(III) during the synthesis process,[19] and most of the Fe units present on the surface of the $CN/CD_3/Fe_6$ composite got dissolved during the irradiation process. The N 1s spectra and C 1s spectral profiles are presented in Figure 8e,f, respectively. The fitting parameters were determined from the XPS spectral profiles (Table 1).[42−46] The N 1s and C 1s spectral profiles were analyzed, and it was observed that the binding energy and percentage of the total area of the functional group after irradiation changed by different degrees. This indicated that the chemical surroundings of C and N were diversified.
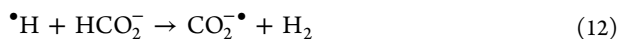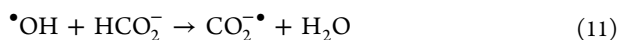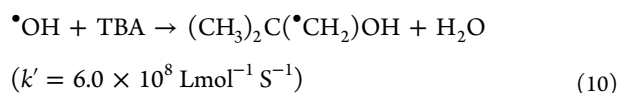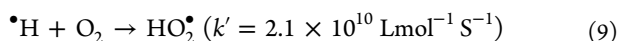
3.4.2. Cyclic Experiment of the $CN/CD_3/Fe_6$ Composite Used for MB Degradation. Before conducting the EBI experiment, the recycled $CN/CD_3/Fe_6$ composite was added to the MB solution with an initial concentration of 500 mg/L. The degradation and mineralization of MB were compared over five cyclic experiments. The iron ion concentration was measured after each experiment to explore the leaching ability of iron ions present on the $CN/CD_3/Fe_6$ composite.

As shown in Figure 9a, the adsorption performance of the $CN/CD_3/Fe_6$ composite changed slightly after five cycles of irradiation at the solid-to-liquid ratio of 10 mg/5 mL.

A small drop in the removal efficiency of MB was observed after irradiation. The $CN/CD_3/Fe_6$ composite exhibited good catalytic activity during MB removal after five cycles; this indicates that the XPS technique may only detect the iron ions on the surface of the $CN/CD_3/Fe_6$ composite, and there are still iron ions inside that can participate the surface reactions. The TOC removal efficiency in MB solution reached 57.3% after the first irradiation cycle. Following this, the efficiency decreased markedly as the number of cycles increased (Figure 9b). As seen in Figure 9c, the $C_{[Fe]}$ in the solution dropped significantly, and this could be attributed to repeated washing

processes after the first irradiation cycle. The results indicated that the solution reactions became weak after the first irradiation cycle. The decreased TOC removal efficiency of MB can be potentially attributed to the solution reactions.

3.5. Role of Various Reactive Species on the Process of MB Degradation. Experiments were carried out under four conditions to elucidate the contribution of the reactive species to the process of MB degradation (Table 2). The N_2 saturated system was taken as the control group. In the O_2 saturated system, O_2 could react with the reductive species (e_{aq}^-, $^\bullet H$) (eqs 8 and 9). $^\bullet OH$ was the main reactive species.[47,48] *Tert*-butanol (TBA) could scavenge $^\bullet OH$ (eq 10), and the main reactive species in the N_2 saturated + TBA system were e_{aq}^-, $^\bullet H$.[49] The primary reactive species present in the N_2 saturated + formate system was e_{aq}^-, and this could be attributed to the reactions occurring between formate and $^\bullet OH$ and $^\bullet H$ (eqs 11 and 12).[22]

$$e_{aq}^- + O_2 \rightarrow {}^\bullet O_2^- \ (k' = 1.9 \times 10^{10} \ \text{Lmol}^{-1} \ \text{S}^{-1}) \tag{8}$$

$$^\bullet H + O_2 \rightarrow HO_2^\bullet \ (k' = 2.1 \times 10^{10} \ \text{Lmol}^{-1} \ \text{S}^{-1}) \tag{9}$$

$$^\bullet OH + TBA \rightarrow (CH_3)_2C({}^\bullet CH_2)OH + H_2O$$

$$(k' = 6.0 \times 10^8 \ \text{Lmol}^{-1} \ \text{S}^{-1}) \tag{10}$$

$$^\bullet OH + HCO_2^- \rightarrow CO_2^{-\bullet} + H_2O \tag{11}$$

$$^\bullet H + HCO_2^- \rightarrow CO_2^{-\bullet} + H_2 \tag{12}$$
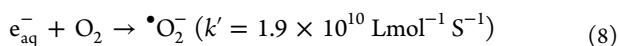
As shown in Figure 10, under conditions of 5 kGy irradiation, the removal efficiency of MB under conditions of the N_2 saturated, O_2 saturated, N_2 saturated + TBA, and N_2 saturated + formate systems reached 94.0, 93.6, 65.8, and 64.5%, respectively. The N_2 saturated system exhibited the maximum removal efficiency for MB. The N_2 saturated system and O_2 saturated system were compared, and little difference in MB removal was observed between the two. This suggests that $^\bullet OH$ is the predominant reactive species during the MB degradation process. The effects of e_{aq}^- and $^\bullet H$ were negligible. The N_2 saturated + TBA system was slightly more efficient than the N_2 saturated + formate system used for MB removal. This indicated that $^\bullet H$ plays an insignificant role in the process of MB degradation. In summary, the contribution of the main reactive species during the MB degradation process was of the order $^\bullet OH > e_{aq}^- > {}^\bullet H$.

It is worth mentioning that the effect of scavenger concentrations on the process of MB degradation using the EBI&CN/CD$_3$/Fe$_6$ system was also explored (Figure S1). The results showed that the concentrations of scavengers used in the experiment did not make a large difference in the MB removal efficiency, indicating that the scavenger concentration of 0.5 M was excessive, and this was enough to consume the target reactive species.

3.6. Mechanism of MB Degradation in the EBI&CN/CD$_3$/Fe$_6$ System. Based on the reported literature[50,51] and the results of the present work, the degradation mechanism of MB in the EBI&CN/CD$_3$/Fe$_6$ system was proposed. Figure 11a presents three routes: (I) The radiolysis of water generates oxidants and reductants, such as $^\bullet OH$, e_{aq}^-, $^\bullet H$, and H_2O_2. (II) The Haber−Weiss reactions between H_2O_2 (produced in situ during the process of water radiolysis) and iron ions in the solution promote the formation of $^\bullet OH$. CDs in the solution can catalyze the decomposition of H_2O_2 to promote the

production of $^\bullet OH$. (III) Finally, H_2O_2 (produced in situ during the process of water radiolysis) adsorbed on the surface of the CN/CD$_3$/Fe$_6$ composite reacts with the CDs of the CN/CD$_3$/Fe$_6$ composite to trigger the production of $^\bullet OH$. Regardless of the pathways (water radiolysis (I), solution reactions (II), or surface reactions (III)), the MB molecules could be degraded by these reactive species. Based on the mechanism presented and the identified intermediates in the MB solution (the *m/z* value of the detected intermediates and the corresponding chemical structures are shown in Table 3), the possible MB degradation pathways were proposed. Two MB degradation pathways were observed (Figure 11b). The first involved the pathway, where the MB molecule was attacked by e_{aq}^- and $^\bullet H$, resulting in the formation of the intermediates I1 (*m/z* = 306) and I2 (*m/z* = 284). For the second pathway, the production of I3 (*m/z* = 301) was attributed to the oxidation of $^\bullet OH$.[52] I4 (*m/z* = 270) and I5 (*m/z* = 256) were produced by eliminating the methyl group by breaking the -N-(CH$_3$)$_2$ bond.[53] I6 (*m/z* = 139) and I7 (*m/z* = 136) were the products of consecutive hydroxylation and ring rupture processes.[54] I3 was continuously attacked by $^\bullet OH$ to form I8 (*m/z* = 202). Following this, it was oxidized to obtain I9 (*m/z* = 158).[55] These intermediates were the products under 2 kGy conditions and were further oxidized and mineralized to form CO_2, H_2O, NO_3^-, SO_4^{2-}, and other low-molecular-weight organics under conditions of large irradiation doses.

It is worth mentioning that the intermediates of MB in the EBI and EBI&CN/CD$_3$/Fe$_6$ system were compared and analyzed. The EBI&CN/CD$_3$/Fe$_6$ system produced fewer intermediates compared to the EBI system, which were all low-molecular-weight substances. It can be inferred that the EBI&CN/CD$_3$/Fe$_6$ system is more favorable to realize the decomposition of the organic dyes to produce small molecules. Thus, the system exhibits a great application value for the mineralization of organic matters.

4. CONCLUSIONS

The degradation mechanism of organic dyes using the EBI&CN/CD$_3$/Fe$_6$ system was systemically studied. The degradation and mineralization of organic dyes were significantly promoted by the addition of CN/CD$_3$/Fe$_6$. The homogeneous irradiation system was more beneficial to realize the degradation of organic dyes than the EBI system since both the Haber−Weiss reactions in the solution and the catalytic role of CDs are the contributing factors for the generation of $^\bullet OH$. There may be surface reactions in the heterogeneous irradiation system to further promote the generation of $^\bullet OH$. The removal efficiency of organic dyes was not significantly affected in the pH range of 3−11, and the CN/CD$_3$/Fe$_6$ composite broadened the pH applicability of Fenton oxidation reactions for organic dyes. Cyclic experiments were conducted to study MB degradation, and the results indicated that the CN/CD$_3$/Fe$_6$ composite exhibited good stability and reusability after five times of irradiation. Results from scavenging experiments revealed that $^\bullet OH$ played the most crucial role during the MB degradation process. A total of nine intermediates produced in the EBI&CN/CD$_3$/Fe$_6$ system were detected using the LC-MS technique, and the possible MB degradation mechanism was proposed. MB could be degraded by the reactive species, which are produced by three reaction pathways (water radiolysis (I), solution reactions (II), or surface reactions (III)); based on the results, two pathways

for the MB degradation were proposed. The results revealed that the EBI&CN/CD$_3$/Fe$_6$ system could be effectively used to treat wastewater containing organic dyes.

ASSOCIATED CONTENT

ⓈⒾ Supporting Information

The Supporting Information is available free of charge at https://pubs.acs.org/doi/10.1021/acsomega.2c00512.

(PDF)

AUTHOR INFORMATION

Corresponding Authors

Long Zhao − State Key Laboratory of Advanced Electromagnetic Engineering and Technology, School of Electrical and Electronic Engineering, Huazhong University of Science and Technology, Wuhan 430074, China; ⓞ orcid.org/0000-0002-6126-2210; Phone: +8615021474065; Email: zhaolong@hust.edu.cn

Miao Yang − School of Chemistry, Chemical Engineering and Life Sciences, Wuhan University of Technology, Wuhan 430070, China; ⓞ orcid.org/0000-0003-4522-772X; Phone: Tel: +8618872256465.; Email: yangmiao@whut.edu.cn

Authors

Wen Li − School of Chemistry, Chemical Engineering and Life Sciences, Wuhan University of Technology, Wuhan 430070, China

Qi Ye − State Key Laboratory of Advanced Electromagnetic Engineering and Technology, School of Electrical and Electronic Engineering, Huazhong University of Science and Technology, Wuhan 430074, China

Tao Xia − School of Chemistry, Chemical Engineering and Life Sciences, Wuhan University of Technology, Wuhan 430070, China

Complete contact information is available at:
https://pubs.acs.org/10.1021/acsomega.2c00512

Author Contributions

§W.L. and Q.Y. contributed equally to this work.

Notes

The authors declare no competing financial interest.

ACKNOWLEDGMENTS

REFERENCES

(1) Bisaria, K.; Sinha, S.; Singh, R.; Iqbal, H. M. N. Recent advances in structural modifications of photo-catalysts for organic pollutants degradation − A comprehensive review. Chemosphere 2021, 284, 131263.

(2) Saravanan, A.; Kumar, P. S.; Jeevanantham, S.; Karishma, S.; Tajsabreen, B.; Yaashikaa, P. R.; Reshma, B. Effective water/wastewater treatment methodologies for toxic pollutants removal: Processes and applications towards sustainable development. Chemosphere 2021, 280, 130595.

(3) Donkadokula, N. Y.; Anand, D.; Kola, K.; Naz, I. A review on advanced physico-chemical and biological textile dye wastewater treatment techniques. Rev. Environ. Sci. Bio/Technol. 2020, 19, 543−560.

(4) Çalık, Ç.; Cifci, D. I. Comparison of kinetics and costs of Fenton and photo-Fenton processes used for the treatment of a textile industry wastewater. J. Environ. Manage. 2022, 304, 114234.

(5) Nie, G.; Hu, K.; Ren, W.; Zhou, P.; Duan, X.; Xiao, L.; Wang, S. Mechanical agitation accelerated ultrasonication for wastewater treatment: Sustainable production of hydroxyl radicals. Water Res. 2021, 198, 117124.

(6) Trojanowicz, M.; Bojanowska-czajka, A.; Szreder, T.; Meczynska-Wielgosz, S.; Bobrowski, K.; Fornal, E.; Nichipor, H. Application of ionizing radiation for removal of endocrine disruptor bisphenol A from waters and wastewaters. Chem. Eng. J. 2021, 403, 126169.

(7) Krishnan, R. Y.; Manikandan, S.; Subbaiya, R.; Biruntha, M.; Govarthanan, M.; Karmegam, N. Removal of emerging micropollutants originating from pharmaceuticals and personal care products (PPCPs) in water and wastewater by advanced oxidation processes: A review. Environ. Technol. Innovation 2021, 23, 101757.

(8) Buxton, G. V.; Greenstock, C. L.; Helman, W. P.; Ross, A. B. Critical Review of rate constants for reactions of hydrated electrons, hydrogen atoms and hydroxyl radicals ($^{\bullet}OH/^{\bullet}O^-$) in Aqueous Solution. J. Phys. Chem. Ref. Data 1988, 17, 513.

(9) Getoff, N. Radiation-induced degradation of water pollutants-state of the art. Radiat. Phys. Chem. 1996, 47, 581−593.

(10) Chen, H.; Wang, J. Degradation of sulfamethoxazole by ozonation combined with ionizing radiation. J. Hazard. Mater. 2021, 407, 124377.

(11) Yang, Q.; Chen, D.; Chu, L.; Wang, J. Enhancement of ionizing radiation-induced catalytic degradation of antibiotics using Fe/C nanomaterials derived from Fe-based MOFs. J. Hazard. Mater. 2020, 389, 122148.

(12) Shah, N. S.; Khan, J. A.; Sayed, M.; Khan, Z. U. H.; Iqbal, J.; Arshad, S.; Junaid, M.; Khan, H. M. Synergistic effects of H_2O_2 and $S_2O_8^{2-}$ in the gamma radiation induced degradation of congo-red dye: Kinetics and toxicities evaluation. Sep. Purif. Technol. 2020, 233, 115966.

(13) Shao, B.; Liu, X.; Liu, Z.; Zeng, G.; Zhang, W.; Liang, Q.; Liu, Y.; He, Q.; Yuan, X.; Wang, D.; Luo, S.; Gong, S. Synthesis and characterization of 2D/0D g-C$_3$N$_4$/CdS-nitrogen doped hollow carbon spheres (NHCs) composites with enhanced visible light photodegradation activity for antibiotic. Chem. Eng. J. 2019, 374, 479−493.

(14) Yang, J.; Song, H.; Zhang, Y.; Zhu, X. Preparation of functionalization graphite carbonitride photocatalytic membrane and its application in degradation of organic pollutants. Surf. Interfaces 2021, 24, 101092.

(15) Bai, X.; Li, M.; Li, J.; Rao, X.; Zheng, S.; Zhang, Y. Graphitic Carbon Nitride Codoped with Sulfur and Yttrium for Efficient Visible-Light Photocatalytic Performance. ACS Appl. Energy Mater. 2021, 4, 14390−14399.

(16) Liu, Z.; Shen, Q.; Zhou, C.; Fang, L.; Yang, M.; Xia, T. Kinetic and Mechanistic Study on Catalytic Decomposition of Hydrogen Peroxide on Carbon-Nanodots/Graphitic Carbon Nitride Composite. Catalysts 2018, 8, 445.

(17) Chen, Z.-y.; Ji, T.; Xu, Z.; Guan, P.; Jv, D. Hydrothermally activated TiO$_2$ nanoparticles with a C-dot/g-C$_3$N$_4$ heterostructure for photocatalytic enhancement. Nanoscale Adv. 2021, 3, 4089−4097.

(18) Yang, M.; Soroka, I.; Jonsson, M. Hydroxyl radical production in aerobic aqueous solution containing metallic tungsten. Catal. Commun. 2015, 71, 93−96.

(19) Fang, L.; Liu, Z.; Zhou, C.; Guo, Y.; Feng, Y.; Yang, M. Degradation Mechanism of Methylene Blue by H_2O_2 and Synthesized Carbon Nanodots/Graphitic Carbon Nitride/Fe (II) Composite. J. Phys. Chem. C 2019, 123, 26921−26931.

(20) Zheng, M.; Bao, Y.; Huang, Z.; Qiu, W.; Xu, G.; Wang, Z. Radiolysis of carbamazepine by electron beam: Roles of transient reactive species and biotoxicity of final reaction solutions on rotifer. *Sci. Total Environ.* **2020**, *703*, 135013.

(21) Changotra, R.; Guin, J. P.; Varshney, L.; Dhir, A. Assessment of reaction intermediates of gamma radiation-induced degradation of ofloxacin in aqueous solution. *Chemosphere* **2018**, *208*, 606−613.

(22) Qiu, H.-B.; Bin, Hu. Y.; Chong, H. J.; Yuan, L.; Sheng, G. P. Degradation and detoxification of 1-butyl-3-methylimidazolium bromide by γ-irradiation in aqueous solution. *Chem. Eng. J.* **2019**, *364*, 440−447.

(23) Arshad, R.; Bokhari, T. H.; Khosa, K. K.; Bhatti, I. A.; Munir, M.; Iqbal, M.; Iqbal, D. N.; Khan, M. I.; Iqbal, M.; Nazir, A. Gamma radiation induced degradation of anthraquinone Reactive Blue-19 dye using hydrogen peroxide as oxidizing agent. *Radiat. Phys. Chem.* **2020**, *168*, 108637.

(24) Ma, X.; Zhou, Y.; Gu, S.; Mei, S.; Zhu, G.; Yu, M.; et al. Degradation of hexavalent chromium and methyl orange by the synergistic system of graphitic carbon nitride and electron beam irradiation. *Chemosphere* **2022**, *287*, 132228.

(25) Chen, X.; Zhuan, R.; Wang, J. Assessment of degradation characteristic and mineralization efficiency of norfloxacin by ionizing radiation combined with Fenton-like oxidation. *J. Hazard. Mater.* **2021**, *404*, 124172.

(26) Chen, X.; Wang, X.; Fang, D. A review on C1s XPS-spectra for some kinds of carbon materials. *Fullerenes, Nanotubes, Carbon Nanoatruct.* **2020**, *28*, 1048−1058.

(27) Chen, Z.; Zhang, J.; Zheng, S.; Ding, J.; Sun, J.; Dong, M.; Abbas, M.; Chen, Y.; Jiang, Z.; Chen, J. The texture evolution of g-C$_3$N$_4$ nanosheets supported Fe catalyst during Fischer-Tropsch synthesis. *Mol. Catal.* **2018**, *444*, 90−99.

(28) Zhang, H.; Li, W.; Yan, Y.; Wang, W.; Ren, Y.; Li, X. Synthesis of highly porous g-C$_3$N$_4$ nanotubes for efficient photocatalytic degradation of sulfamethoxazole. *Mater. Today Commun.* **2021**, *27*, 102288.

(29) Yadav, A. A.; Kang, S.; Hunge, Y. M. Photocatalytic degradation of Rhodamine B using graphitic carbon nitride photocatalyst. *J. Mater. Sci.: Mater. Electron.* **2021**, *32*, 15577−15585.

(30) Prabakaran, E.; Velempini, T.; Molefe, M.; Pillay, K. Comparative study of KF, KCl and KBr doped with graphitic carbon nitride for superior photocatalytic degradation of methylene blue under visible light. *J. Mater. Res. Technol.* **2021**, *15*, 6340−6355.

(31) Banerjee, D.; Bhowmick, P.; Pahari, D.; Santra, S.; Sarkar, S.; Das, B.; Chattopadhyay, K. Pseudo first ordered adsorption of noxious textile dyes by low-temperature synthesized amorphous carbon nanotubes. *Phys. E* **2017**, *87*, 68−76.

(32) Mahamallik, P.; Pal, A. Photo-Fenton process in Co(II)-adsorbed admicellar soft-template on alumina support for methyl orange degradation. *Catal. Today* **2020**, *348*, 212−222.

(33) Zhuan, R.; Wang, J. Degradation of sulfamethoxazole by ionizing radiation: Kinetics and implications of additives. *Sci. Total Environ.* **2019**, *668*, 67−73.

(34) Sun, X.; Xu, D.; Dai, P.; Liu, X.; Tan, F.; Guo, Q. Efficient degradation of methyl orange in water via both radical and non-radical pathways using Fe-Co bimetal-doped MCM-41 as peroxymonosulfate activator. *Chem. Eng. J.* **2020**, *402*, 125881.

(35) Sun, M.; Chu, C.; Geng, F.; Lu, X.; Qu, J.; Crittenden, J.; et al. Reinventing Fenton Chemistry: Iron Oxychloride Nanosheet for pH-Insensitive H$_2$O$_2$ Activation. *Environ. Sci. Technol. Lett.* **2018**, *5*, 186−191.

(36) Alnajrani, M. N.; Alsager, O. A. Decomposition of DNA staining agent ethidium bromide by gamma irradiation: Conditions, kinetics, by-products, biological activity, and removal from wastewater. *J. Hazard. Mater.* **2020**, *389*, 122142.

(37) Wang, M.; Cui, S.; Yang, X.; Bi, W. Synthesis of g-C$_3$N$_4$/Fe$_3$O$_4$ nanocomposites and application as a new sorbent for solid phase extraction of polycyclic aromatic hydrocarbons in water samples. *Talanta* **2015**, *132*, 922−928.

(38) Ma, T.; Shen, Q.; Zhao, B.; Xue, J.; Guan, R.; Liu, X.; Jia, H.; Xu, B. Facile synthesis of Fe-doped g-C$_3$N$_4$ for enhanced visible-light photocatalytic activity. *Inorg. Chem. Commun.* **2019**, *107*, 107451.

(39) Liu, Z.; Guo, W.; Liu, X.; Wu, G.; Tang, Y.; Mo, Z.; Yang, D. Study on photoelectric properties of Fe-Co codoped g-C$_3$N$_4$. *Chem. Phys. Lett.* **2021**, *781*, 138951.

(40) Ji, S.; Yang, Y.; Zhou, Z.; Li, X.; Liu, Y. Photocatalysis-Fenton of Fe-doped g-C$_3$N$_4$ catalyst and its excellent degradation performance towards RhB. *J. Water Process Eng.* **2021**, *40*, 101804.

(41) Asadzadeh-Khaneghah, S.; Asadzadeh-khaneghah, S.; Habibi-Yangjeh, A.; Habibi-yangjeh, A.; Seifzadeh, D.; Chand, H. Visible-light-activated g-C$_3$N$_4$ nanosheet/carbon dot/FeOCl nanocomposites: Photodegradation of dye pollutants and tetracycline hydrochloride. *Colloids Surf., A* **2021**, *617*, 126424.

(42) Zhang, J.; Zhao, Y.; Wu, A. L.; Li, J.; Wang, Y. X. Ni(OH)$_2$/Ni/g-C$_3$N$_4$ composite: An efficient electrocatalyst for hydrogen evolution. *J. Fuel Chem. Technol.* **2021**, *49*, 198−204.

(43) Narkbuakaew, T.; Sattayaporn, S.; Saito, N.; Sujaridworakun, P. Investigation of the Ag species and Synergy of Ag-TiO$_2$ and g-C$_3$N$_4$ for the Enhancement of Photocatalytic Activity under UV-Visible Light Irradiation. *Appl. Surf. Sci.* **2022**, *573*, 151617.

(44) Liu, M.; Niu, B.; Guo, H.; Ying, S.; Chen, Z. Simple preparation of g-C$_3$N$_4$@Ni$_3$C nanosheets and its application in supercapacitor electrode materials, hydrogengeneration via NaBH$_4$ hydrolysis and reduction of p−nitrophenol. *Inorg. Chem. Commun.* **2021**, *130*, 108687.

(45) Biesinger, M. C.; Payne, B. P.; Grosvenor, A. P.; Lau, L. W. M.; Gerson, A. R.; Smart, R. S. C. Resolving surface chemical states in XPS analysis of first row transition metals, oxides and hydroxides: Cr, Mn, Fe, Co and Ni. *Appl. Surf. Sci.* **2011**, *257*, 2717−2730.

(46) Ma, L.; Wiame, F.; Maurice, V.; Marcus, P. New insight on early oxidation stages of austenitic stainless steel from in situ XPS analysis on single-crystalline Fe−18Cr−13Ni. *Corros. Sci.* **2018**, *140*, 205−216.

(47) Chen, D.; Chu, L.; Wang, J.; Yang, Z.; Yang, Q.; Shen, Y. Degradation of antibiotic cephalosporin C in aqueous solution and elimination of antimicrobial activity by gamma irradiation. *Chem. Eng. J.* **2019**, *374*, 1102−1108.

(48) Chen, X.; Wang, J. Degradation of norfloxacin in aqueous solution by ionizing irradiation: Kinetics, pathway and biological toxicity. *Chem. Eng. J.* **2020**, *395*, 125095.

(49) Zhuan, R.; Wang, J. Degradation of diclofenac in aqueous solution by ionizing radiation in the presence of humic acid. *Sep. Purif. Technol.* **2020**, *234*, 116079.

(50) Yang, M.; Zhang, X.; Grosjean, A.; Soroka, I.; Jonsson, M. Kinetics and Mechanism of the Reaction between H$_2$O$_2$ and Tungsten Powder in Water. *J. Phys. Chem. C* **2015**, *119*, 22560−22569.

(51) Alkhuraiji, T. S. Effect of Co60 irradiation on the degradation and mineralization of sulfonated aromatic compounds in aqueous solutions. *Chemosphere* **2019**, *228*, 769−777.

(52) Su, S.; Liu, Y.; Liu, X.; Jin, W.; Zhao, Y. Transformation pathway and degradation mechanism of methylene blue through b-FeOOH@GO catalyzed photo-Fenton-like system. *Chemosphere* **2019**, *218*, 83−92.

(53) Nguyen, C. H.; Fu, C.; Juang, R. Degradation of methylene blue and methyl orange by palladium-doped TiO$_2$ photocatalysis for water reuse: Efficiency and degradation pathways. *J. Cleaner Prod.* **2018**, *202*, 413−427.

(54) Wolski, L.; Ziolek, M. Insight into pathways of methylene blue degradation with H$_2$O$_2$ over mono and bimetallic Nb, Zn oxides. *Appl. Catal., B* **2018**, *224*, 634−647.

(55) Yu, X.; Zhang, J.; Chen, Y.; Ji, Q.; Wei, Y.; Niu, J.; et al. Ag-Cu$_2$O composite films with enhanced photocatalytic activities for methylene blue degradation: Analysis of the mechanism and the degradation pathways. *J. Environ. Chem. Eng.* **2021**, *9*, 106161.